Check for updates

Proceedings of the ASME 2025 Heat Transfer Summer Conference
HT2025
July 8-10, 2025, Westminster, CO

HT2025-156849

Downloaded from http://asmedigitalcollection.asme.org/HT/proceedings-pdf/HT2025/88988/V001T03A006/7542844/v001t03a006-ht2025-156849.pdf by University of California Library - Berkeley user on 30 December 2025

MACHINE LEARNING COMBINED IMAGE AND SENSOR DATA ANALYSIS OF TWO-PHASE MORPHOLOGY AND HEAT TRANSFER DATA FOR DROPLET VAPORIZATION ON A SURFACE AT NEAR CRITICAL HEAT FLUX CONDITIONS

Ursan Tchouteng Njike, Anisa Silva and Van P. Carey
Mechanical Engineering Department
University of California at Berkeley

ABSTRACT

For droplet vaporization on a superheated hydrophilic surface, earlier studies have demonstrated that use of machine learning tools to analyze both image information from high-speed video and digital data from sensors can be an effective path to understanding the physics and developing a useful model to predict performance when the surface superheat is at low to moderate levels. For such conditions, the two-phase morphology of the system is usually well-behaved, exhibiting conduction-dominated film evaporation of the spread droplet, or nucleate boiling at active nucleation sites in the liquid film of the spread droplet. At higher surface superheat levels, experiments have shown that the droplet vaporization process becomes chaotic, with the process alternating between rapid vaporization of liquid in contact with the surface and ejection of liquid off the surface by strong vapor recoil forces. For our experiments with water droplets at atmospheric pressure, this regime corresponds to superheat levels ranging from about 35 to 55 deg. C. At the low superheat end of this regime, extremely high mean heat flux levels are achieved, but as superheat further increases, less of the surface stays wetted due to the increasing vapor recoil forces, and heat flux begins to decrease as the boiling process becomes like transition pool boiling with progressively less of the surface in contact with liquid. This exploration of the use of a specialized convolution neural network (CNN) to simultaneously analyze high speed video images and digital data for this high-superheat, near-critical-heat-flux regime of droplet vaporization is of special interest for two reasons. First, this vaporization regime results in high heat flux levels that make it attractive for high heat flux cooling for high-powered electronics. Use of machine learning tools to learn more about the mechanisms of this vaporization regime may open the door to new high flux thermal management technologies. In addition, because of its complexity, the two-phase morphology of the vaporization process in this regime is expected to be a very challenging task for CNN machine learning tools. In this study we conducted deposited water droplet spreading and vaporization experiments that captured digital data input (measured surface superheat, mean heat flux during the vaporization process, wetting contact angle, droplet size, etc.) and images of the droplet vaporization two-phase morphology from high-speed video during each experiment. This paper summarizes our successful development of a specialized hybrid CNN design that is trained using the combination of digital measurements and images obtained in our experiments. This CNN design provides deep insight into correlation between the two-phase morphology and heat transfer performance for this near critical heat flux vaporization regime. It also provides a pathway to a heat transfer performance model that fits the performance data to a high level of agreement. Using data collected from the droplet deposition experiment, this network design has been trained to predict the mean heat flux with a root mean square percent error of only about 2.0% and 8.0% on a training and testing dataset respectively. The hybrid network developed in this research appears to be a promising strategy for analyzing experimental data for physical systems with complex morphology that are best investigated experimentally with a combined use of imaging and digital sensor instrumentation.

Keywords: Droplet vaporization, nucleate boiling, nanostructured surface, convolution neural network, digital and image data analysis.

NOMENCLATURE

A	droplet mean footprint area during vaporization
f	camera frames per second
h_{lv}	latent heat of vaporization
$\bar{\dot{q}}$	mean heat flux during droplet vaporization
V_0	droplet initial volume
ρ	liquid water density

Copyright © 2025 by ASME

1. INTRODUCTION

The study summarized in this paper was an exploration of how a specialized machine-learning analysis approach could be used to enhance research on the vaporization physics of liquid water droplets deposited on nanostructured surfaces when surface superheat levels are approaching the maximum heat flux conditions. Since research in this area generally involves collecting digital data from sensors and observation or imaging of the two-phase morphology, this study specifically sought to consider machine learning approaches that can simultaneously analyze both digital data and image information.

A micrograph of the nanostructured surface type considered here is shown in Figure 1. Earlier investigations of pool boiling and droplet vaporization on surfaces of this type have indicated that droplet vaporization on these surfaces exhibits distinct regimes of heat transfer, similar to those for pool boiling. Figure 2 illustrates the correspondence between droplet vaporization regimes and pool boiling regimes documented in the experimental studies summarized by Carey, et al. [1].

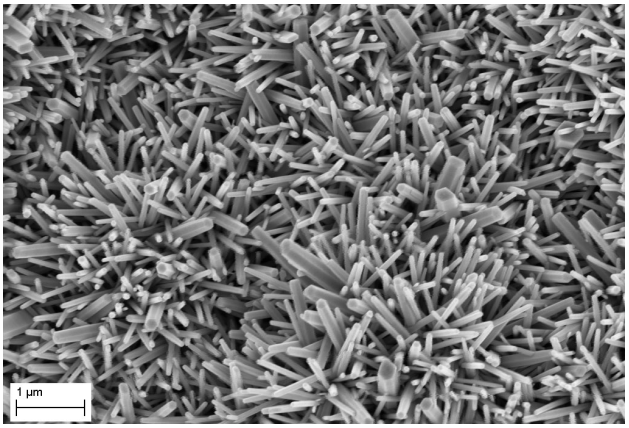

Fig. 1. A micrograph of the nanostructured surface.

Vaporization of water droplets deposited on the nanoporous surface shown in Fig. 1 is of interest because the surface is hydrophilic, exhibiting a contact angle less than 10 degrees and the surface exhibits extreme wicking. At low to moderate surface superheat levels, this causes impinging droplets to spread rapidly after first contact to form a very thin liquid film with a large footprint. The subsequent vaporization of the liquid film occurs rapidly, resulting in a high mean heat flux during the vaporization process.

The traditional approach used in experimental studies of boiling processes or impinging droplet vaporization has been to collect digital data measurements such as surface temperature, system pressure, surface contact angle, wicking speed, impingement velocity, etc., and either visual observations or imaging of the system during the process with high speed still photography or high-speed video. In the past five years there have been a number of investigations that have explored how digital data for different types of boiling processes can be analyzed and/or predictive models can be developed using machine learning tools. Many of these investigations explored the use of data based neural network models (see, for example, [2-13]), while other recent studies (e.g., [14-17]) have used genetic algorithms and other methodologies. These investigations have demonstrated that machine learning tools can offer very useful alternative ways to enhance analysis and modeling of digital data trends in boiling research.

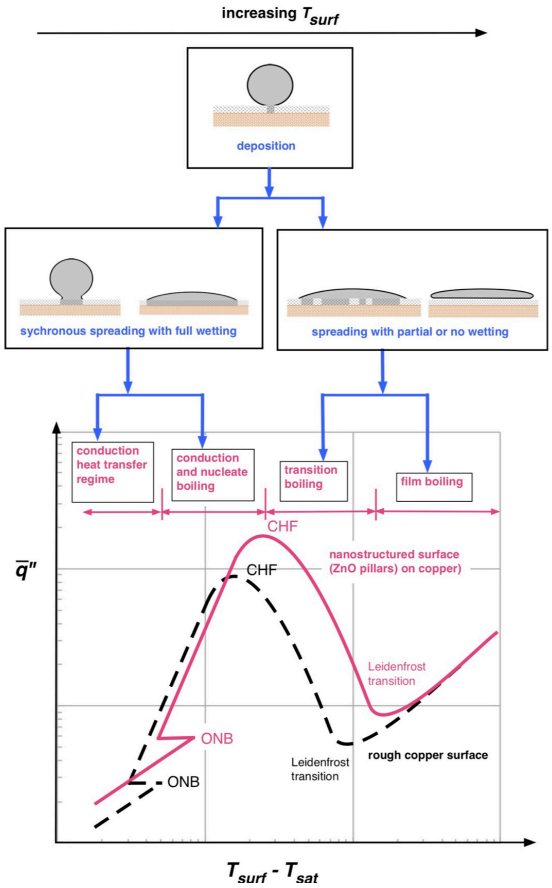

Fig. 2. Droplet vaporization regimes and pool boiling regimes correspondence.

If an imaging system records an image of the two-phase boiling system at the instant the digital data is recorded, this results in data sets like that depicted in Fig. 3, with each data point consisting of a collection of digital values of system parameters, and a corresponding system image.

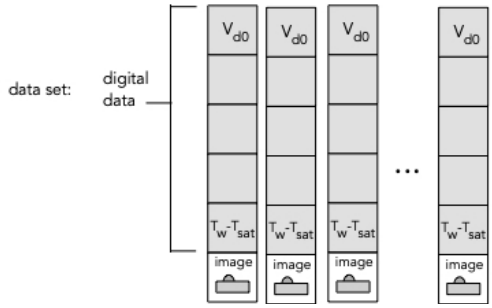

Fig. 3. Typical combined digital and image information from boiling/vaporization experiments.

Copyright © 2025 by ASME

Downloaded from http://asmedigitalcollection.asme.org/HT/proceedings-pdf/HT2025/88988/V001T03A006/7542844/v001t03a006-ht2025-156849.pdf by University of California Library - Berkeley user on 30 December 2025

Many previous studies of this type have collected combined digital data and image information about the process in this way under widely varying conditions. It is noteworthy, however, that until very recently, the correlation of image information with expected morphology regimes and digital measured parameter trends was usually established through manual comparisons of image features. This approach established the now well-known combinations of boiling liquid-vapor morphology features that correspond to the isolated bubble regime, the regime of slugs and bubbles (incipient CHF regime), the transition boiling regime, and the film boiling regime.

The recent availability of convolution neural networks (CNN's) to analyze information content in images has opened the door to using CNN's to analyze images captured during boiling processes. Developed in the 1980s, convolution neural networks are now commonly used as the backbone of many computer vision applications. These applications range from self-driving vehicles to medical image analysis, facial recognition, and more. Recent studies of boiling heat transfer have explored ways to leverage this powerful tool to better understand boiling processes. The paper of Yang, et al. [18] discusses the use of high-speed camera visualization to examine flow boiling in microchannels. The study aims to use a CNN model to identify the flow pattern for use as a means of an accurate heat transfer mechanism prediction for applications. To achieve an optimized performance, the image was pre-processed to address issues related to unbalanced lighting and other effects that may not be relevant to the classification of pattern flow. In another similar study, Lee [19] explored strategies to optimize experimental observation and measurements of pool boiling heat transfer using computer vision techniques. The computer vision applied in that study performs bubble detection and segmentation to track bubble movements as they depart from the surface. This helps in capturing key performance parameters such as bubble density, size, and departure frequency autonomously.

Most commonly, CNN analysis of boiling process images has been done in parallel with an analysis to fit a physics-based model, or a machine learning model (such as a neural network), to the digital data from the experiment. Because past research has established a correlation between superheat level and boiling regimes, separate CNN model analysis of boiling regimes and two-phase morphology have frequently postulated to be functions primarily of superheat. If this postulated connection is adopted, training of a CNN model that predicts superheat from image features is straightforward, and in cases where the image features are strongly correlated to superheat alone, the CNN model can achieve a good fit to the data.

The work summarized here focuses on the vaporization/boiling process associated with liquid water droplet depositions on a superheated surface described above. In an earlier investigation, Carey, et al. [1] assessed regime changes by examining measured surface superheat droplet size, and surface wetting data together with high-speed videos of the droplet vaporization process in their experiments. Their high-speed videos provided visual evidence of the variation of the two-phase morphology as surface superheat, droplet size and surface wetting varied. Observations and data from this earlier study indicate two important points related to the study summarized here. First, the earlier study documented that, for water droplet vaporization at atmospheric pressure, the mean heat flux depends on surface superheat, surface wetting (contact angle), initial droplet size, the morphology of the liquid, and the presence or absence of nucleate boiling at locations on the heating surface during experiments. This indicates that the liquid morphology varies with operating conditions and properties. In general, the morphology is mainly affected by pressure and surface superheat. However, in our current study, the system pressures are fixed for all the droplet deposition experiments since they were conducted at atmospheric pressure. As discussed above, for a legacy-type study, the operating conditions and surface parameters on the left affect heat transfer performance directly, and/or they affect morphology. The second relevant point from this earlier study is that it indicates that the boiling features of vaporization of deposited water droplets on superheated surfaces are strongly similar to those for pool boiling observed in quenching experiments under similar conditions. Droplet deposition experiments therefore can be used to explore nucleate boiling mechanisms near the onset of nucleate boiling while providing imaging access close to the surface, which allows more effective use of optical methods to obtain image information about the process.

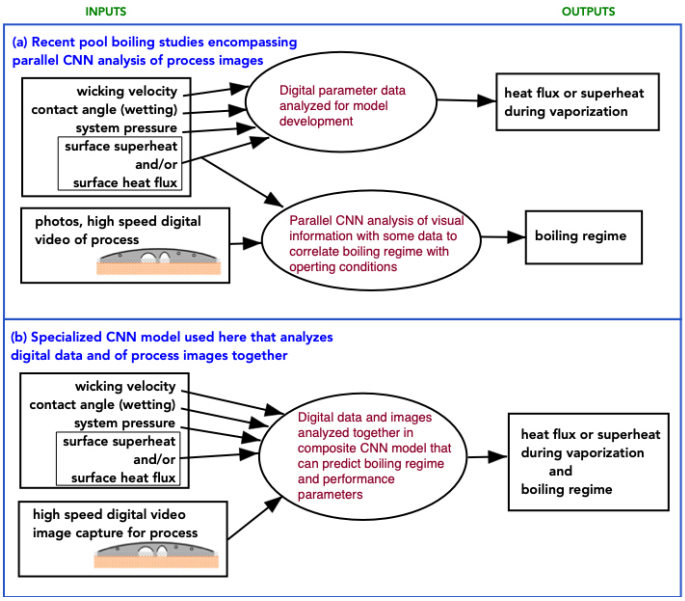

Fig. 4. Categories in the evolution of morphology assessment in experimental strategies.

The earlier experimental study of Carey, et al. [1] explored water droplet vaporization on superheated surfaces by extracting digital information from video frame images, as traditionally done in legacy studies. In a very recent study [20], the authors explored an alternative approach that used machine learning to

Downloaded from http://asmedigitalcollection.asme.org/HT/proceedings-pdf/HT2025/88988/V001T03A006/7542844/v001t03a006-ht2025-156849.pdf by University of California Library - Berkeley user on 30 December 2025

Copyright © 2025 by ASME

directly extract information from video images using a customized Convolution Neural Network (CNN) that simultaneously analyzes digital data and images. Note that while other investigators have explored machine learning of boiling images independently in parallel with digital data analysis (depicted in Fig. 4a), our earlier investigation explored using a CNN model to analyze a combined information flow of digital data and concurrent images (depicted in Fig. 4b). That study demonstrated that this approach offered two advantages. One is that image captured records of morphology are strongly correlated with surface superheat and heat transfer and a trained model of this type can be used as a temperature sensor by predicting surface superheat from an input image.

This study also demonstrated that training a specialized CNN model using both measured digital superheat data and corresponding image data can produce a model for predicting heat flux that provides more accurate predictions of surface heat flux compared with models based on measured superheat alone. That study, however, considered water droplet vaporization processes up to surface superheat levels of about 40°C to explore whether the specialized CNN image analysis could distinguish morphologies for conduction dominated, isolated bubble nucleate boiling, and vigorous nucleation boiling. The superheat range above 40 °C is characterized by two mechanisms that are not present at lower superheat levels: (1) local dryout in the spread droplet due to rapid vaporization at bubble nucleation sites, and (2) vapor recoil forces that can eject liquid way from the surface. These mechanisms result in more complex two-phase morphologies, making their use in CNN training more challenging. The goal of the investigation summarized here was to explore use of the specialized CNN network model developed in our previous investigation [ref] to a water droplet vaporization data and morphology image collection that includes the lower superheat data from our previous study, and new data and images for the partial dryout, vapor recoil (PDVR) regime at superheat levels up to 50 °C. The details of the design and training of the specialized CNN model, and the assessment of its use for data in this extensive superheat range are described in the following sections.

2. METHODS: EXPERIMENTAL DATA

2.1 Data Collection

The data used in this study was collected via a droplet deposition experiment. A surface that exhibits a particular contact angle θ and wicking speed is coated on the top of a cylindrical copper rod measuring 2.5 cm in Diameter. The contact angles of water on the coated surfaces were measured using a spherical cap model. On the side of the rod, about 1 mm from the top, two holes are drilled opposite to each other for the insertion of a thermocouple for temperature measurements. This rod is placed on a hot plate with mineral wool insulation of about 1 cm thick on the sides to ensure an adiabatic process. The hot plate is adjusted to a temperature above the nucleation temperature of water. Thermocouples are inserted in the adequate holes of the cylindrical rod closer to the top, where the

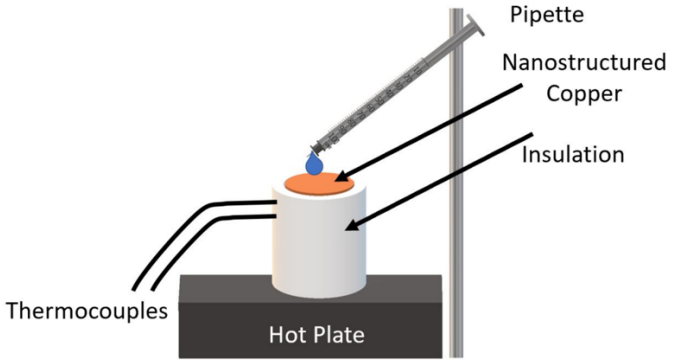

Fig. 5. Droplet Deposition Experiment.

droplet is deposited. These thermocouple temperature readings are used to define the wall superheat temperatures. The droplet sizes are measured using a pipette at the time of deposition. A high-speed camera is placed above the rod to capture the droplet boiling process. The experiment tracks the image, superheat temperature, droplet size, and contact angle as input data. The experiment also tracks the regime classification and heat flux as output data. A schematic of the droplet experiment is shown in Fig. 5. The mean heat flux was calculated using Eq. (1). This equation only involves the latent heat needed to transform the droplet into steam. The energy used to raise the temperature of the droplet to saturation was ignored since it is negligible when compared to the latent heat. In this equation, $\bar{q}$ is the mean heat flux, ρ is the density of water, V_0 is the initial volume of the droplet, h_{lv} is the latent heat of vaporization of water, f is the framerate of the camera, A is the average wetted area, and n is the number of frames between the droplet getting in contact with the surface and its complete evaporation. The frame rate of the camera used in this study was 1200 frames per second. The maximum droplet wetted area was first measured using high speed videos of the droplet vaporization experiments for all test cases. Each video was stepped through until the frame where the footprint of the droplet was largest, this frame was captured and imported to ImageJ where this maximum wetted area was measured. The average wetted area is then taken as 1/2 the maximum wetted area as it is assumed that when the vaporization process completes, the area will go to zero.

$$\bar{\dot{q}} = \frac{\rho V_0 \, h_{lv} f}{nA} \tag{1}$$

Digital and image data were collected from this experiment. The images were selected based on their information richness, i.e. presence of bubbles or gradual shrink, as captured by the camera. A sample of the image data collected is shown in Table 1 for the different morphology considered in this study. This table shows images for different droplet sizes at distinct superheat temperatures. 416 image data were generated from this experiment. This data was split into two sets. 15% of the image data was retained as a test set to evaluate the accuracy of the model on unseen data. The remaining 85% of the image data were augmented using a set augmentation parameter. The

Copyright © 2025 by ASME

Downloaded from http://asmedigitalcollection.asme.org/HT/proceedings-pdf/HT2025/88988/V001T03A006/7542844/v001t03a006-ht2025-156849.pdf by University of California Library - Berkeley user on 30 December 2025

Table 1. Droplet Deposition Image Data of Different Droplet Sizes for each Regime Considered. ΔT is the wall superheat $T_w - T_{sat}$.

Conduction	Isolated Bubble	Vigorous Nucleation	PDVR
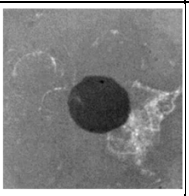 Size = 5 μLΔT = 5K	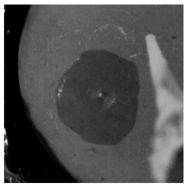 Size = 5 μLΔT = 20K	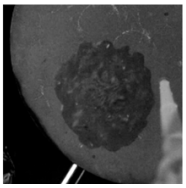 Size = 5 μLΔT = 35K	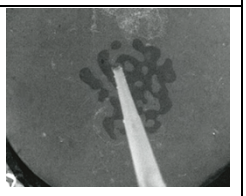 Size = 5 μLΔT = 45K
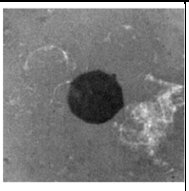 Size = 6 μLΔT = 5K	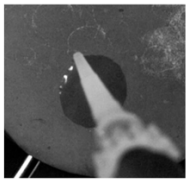 Size = 6 μLΔT = 20K	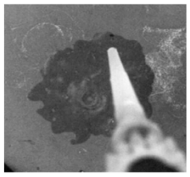 Size = 6 μLΔT = 35K	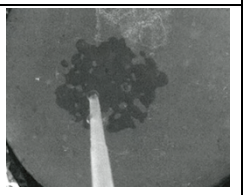 Size = 6 μLΔT = 45K
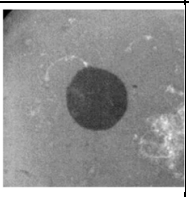 Size = 7 μLΔT = 5K	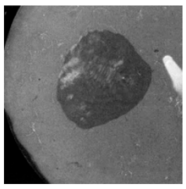 Size = 7 μLΔT = 20K	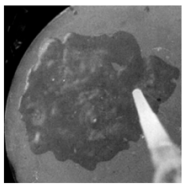 Size = 7 μLΔT = 35K	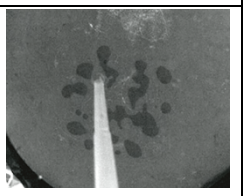 Size = 7 μLΔT = 45K
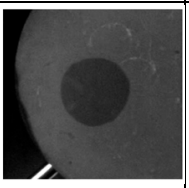 Size = 8 μLΔT = 5K	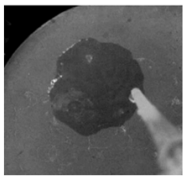 Size = 8 μLΔT = 20K	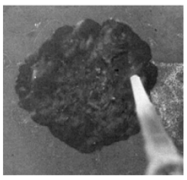 Size = 8 μLΔT = 35K	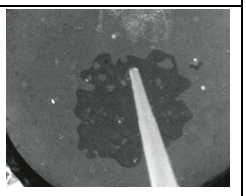 Size = 8 μLΔT = 45K

parameter of the augmentation generator includes random rotation of up to 5 degrees. It also includes horizontal shift, vertical shift, shear, and zoom of up to 10%. Random horizontal flips were allowed to be performed on the images as well. Empty spaces due to the image modification were filled using the nearest pixel value strategy. The purpose of the data augmentation is to help in generating a robust model by deliberately adding perturbation to the image data. This is a common approach as discussed by Connor Shorten & Taghi M. Khoshgoftaar in A survey on Image Data Augmentation for Deep Learning [21]. The data augmentation resulted in a set of 9178 images augmented from 353 of the original images randomly chosen for model training purposes. These input images as well as all the other values used in training the model were preprocessed to eliminate unwanted bias toward higher magnitude values. The images were normalized by dividing the pixel values by 255. This ensured that arrays representing images only have values in the range of 0 to 1. The superheat temperature, droplet size, and contact angle data are normalized by dividing by their respective median values. The regime morphology classification is converted to numerical value via one hot encoding. Since the coloration of the image does not carry a physical interpretation in this experiment, all the original images were converted to grayscale. This conversion significantly reduces the computational cost for training the model since it deals with only one layer array representing the image. The images are then rescaled to 100x100 pixels to further reduce computational cost. At this resolution, most of the important features of the image are still preserved. Table 2 shows the range of data values captured during the experiments.

Table 2. Range of Parameter Values in this Study.

Variable	Range
Superheat Temperature	10 – 50 [K]
Droplet Size	5 – 8 [μL]
Contact Angle	4.41 - 5.07 [°]
Mean Heat Flux	17.7 – 156.4 [W/cm^2]

Table 3. Model Cases Highlighting the Inputs and Outputs Considered

Case I	Case II
Input: - Image Data - Initial Droplet Size - Contact Angle	Input: - Image Data - Initial Droplet Size - Contact Angle - Superheat Temperature
Output: - Mean Heat Flux - Superheat Temperature	Output: - Mean Heat Flux - Nucleation Regime

Network Architecture

Two cases were examined to understand CNN's potential in levering image features for improved mean heat flux prediction. The two cases are summarized in Table 3. Case I examines the

Copyright © 2025 by ASME

Downloaded from http://asmedigitalcollection.asme.org/HT/proceedings-pdf/HT2025/88988/V001T03A006/7542844/v001t03a006-ht2025-156849.pdf by University of California Library - Berkeley user on 30 December 2025

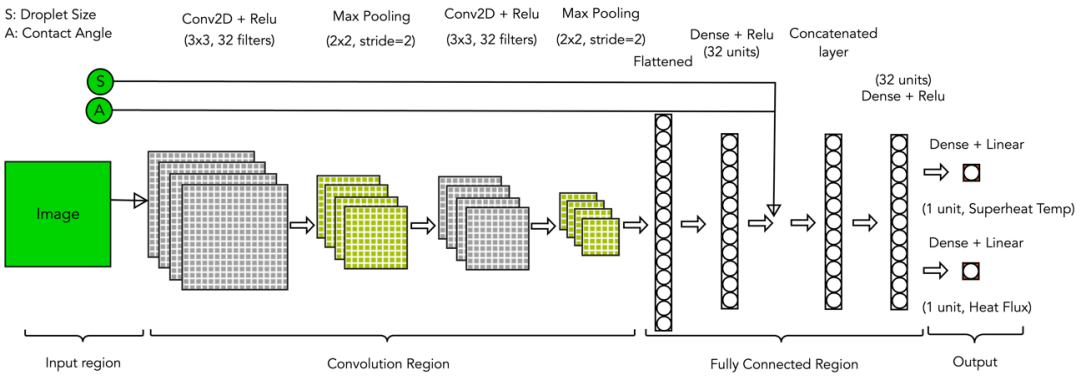

Fig. 6. CNN Architecture for Case I.

(a)

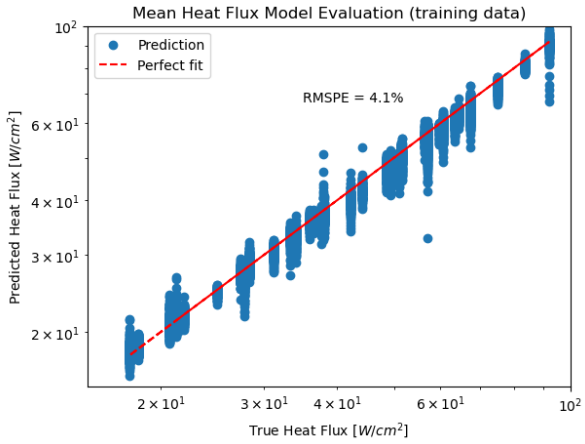

(b)

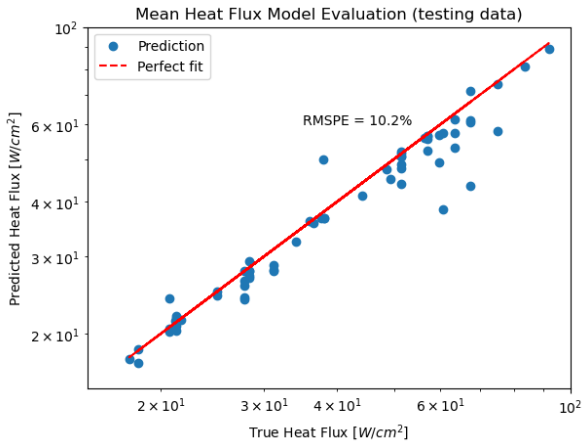

Fig. 7. Mean Heat Flux Prediction Results for Case I on (a) Training Dataset and (b) Testing Dataset.

architecture with information unrelated to the temperature of the system. Case II examines the architecture considering both the appearance of the droplet and the temperature of the system.

2.1.1 Case I

In this section, the objective is to evaluate how well a model can predict the mean heat flux using only droplet size, contact angle, and image information. Note that this includes image morphology information and excludes direct information about the system's temperature. The resulting architecture developed for this case is depicted in Fig. 6. This architecture is configured to take a 100x100 array representation of the image data, the droplet size variable, and the contact angle variable as input, and

(a)

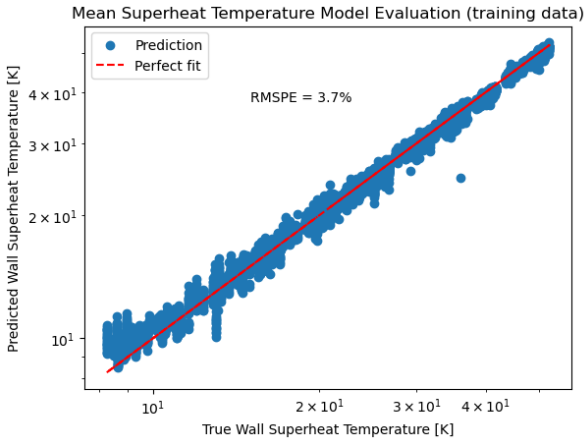

(b)

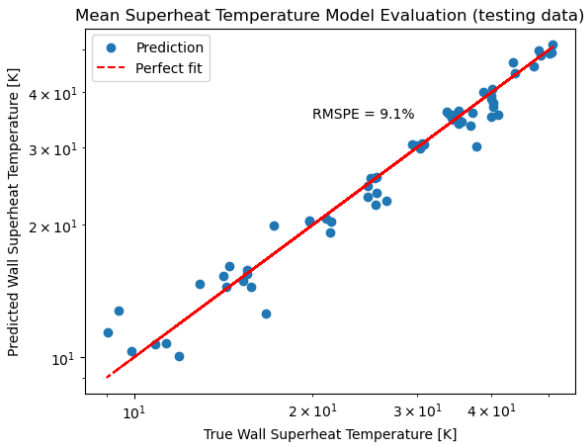

Fig. 8. Superheat Temperature Prediction for Case B on (a) Training and (b) Testing Dataset.

Downloaded from http://asmedigitalcollection.asme.org/HT/proceedings-pdf/HT2025/88988/V001T03A006/7542844/v001t03a006-ht2025-156849.pdf by University of California Library - Berkeley user on 30 December 2025

Copyright © 2025 by ASME

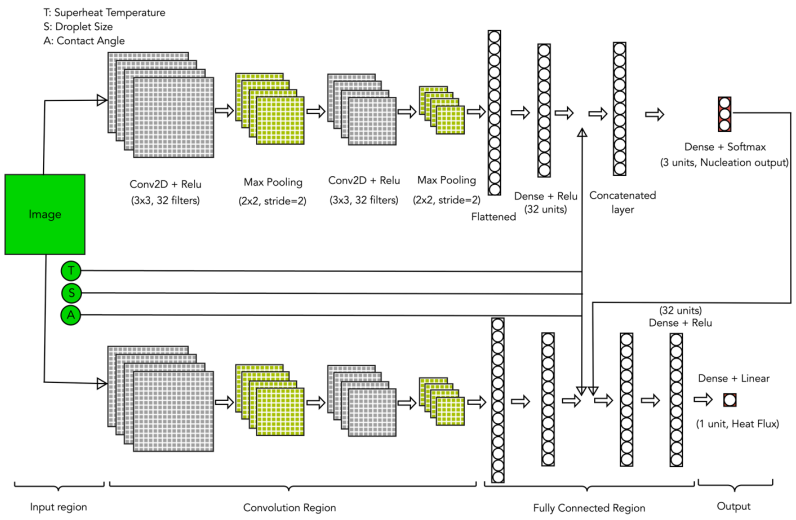

Fig. 9. CNN Architecture for Case II.

(a)

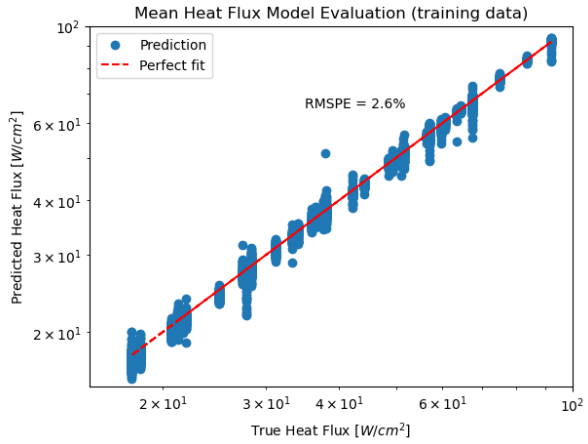

(b)

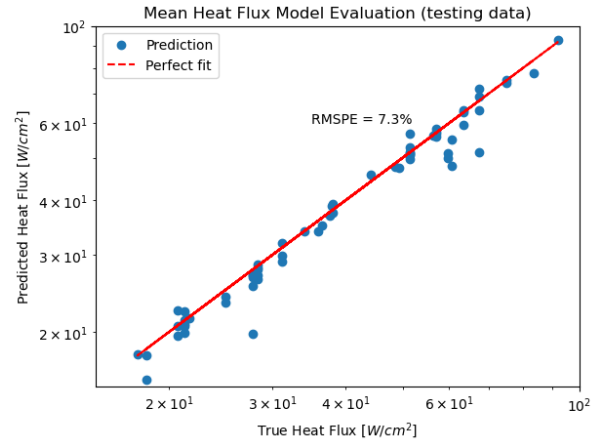

Fig. 10. Mean Heat Flux Prediction results for Case II on (a) Training and (b) Testing Dataset.

it generates the wall superheat temperature and mean heat flux as output. The image data passes through a 3x3 convolution layer with 32 filters and a same padding. From here, a ReLU activation function is applied to this convolution output to introduce non-linearity. A 2x2 max pooling with a stride of 2 and a same padding is applied to summarize the feature captured by the convolution layer. This set of three operations is repeated one more time. As the data enters the fully connected region, the output from the convolution region is flattened. From here it passes through a dense layer with 32 neurons and a ReLU activation function. A skip connection is applied to concatenate the droplet size and contact angle input to the dense layer output. The concatenated data flows through another dense layer with 32 neurons and a ReLU activation function. From here, the data is connected to the 2 final dense layers with one neuron outputting the superheat temperature and mean heat flux. The result from training a model with this architecture is shown in Fig. 7 for the mean heat flux. The RMSPE was evaluated on both the training and testing datasets and was found to be 4.1% and 10.2% respectively. This result demonstrates that the model had strong predictive capability and that the model was able to capture features in the image data to generate predictions. From this result, it is suggested that the model might also accurately predict the superheat temperature. Figure 8 shows the comparison between the superheat temperature prediction against its true value both for the training and testing datasets.

The model also had accurate superheat temperature predictions for both the training and testing datasets with a RMSPE of 3.7% and 9.1% respectively. One may inquire whether having both droplet appearance and temperature information as input data could generate better predictions. This question is answered by training a model on Case II's architecture.

2.1.2 Case II

In this section, the focus is to explore whether combining information about the droplet appearance and the physical condition of the system can generate the strongest results among all cases. Figure 9 is the resulting architecture used in Case II. The CNN architecture here is a replica of the one found to work well for simulated images with a few adjustments to account for desired input and output configurations. Note that Case II's architecture consists of 4 inputs, a 100x100 array representing the image, wall superheat temperature, droplet size, and contact angle. In addition, the output structure in Case II consists of a nucleation regime with four classes and a mean heat flux. Every other part of the architectural structure for Case II was kept the same as the one used for the model simulation. The comparison of the trained model heat flux predictions versus the data values for Case II is depicted in Fig. 10.

The RMSPE was evaluated on both the training and testing datasets and was found to be 2.6% and 7.3% respectively. This result clearly shows an improved prediction accuracy as

Downloaded from http://asmedigitalcollection.asme.org/HT/proceedings-pdf/HT2025/88988/V001T03A006/7542844/v001t03a006-ht2025-156849.pdf by University of California Library - Berkeley user on 30 December 2025

Copyright © 2025 by ASME

compared to the result obtained in Case I for predicting the mean heat flux. From this result, it is believed that the model should also produce highly accurate morphology predictions. Figure 11 summarizes this prediction on both the training and testing datasets. It shows that the model predicts morphologies for all the images in the entire training dataset with 100% accuracy. The

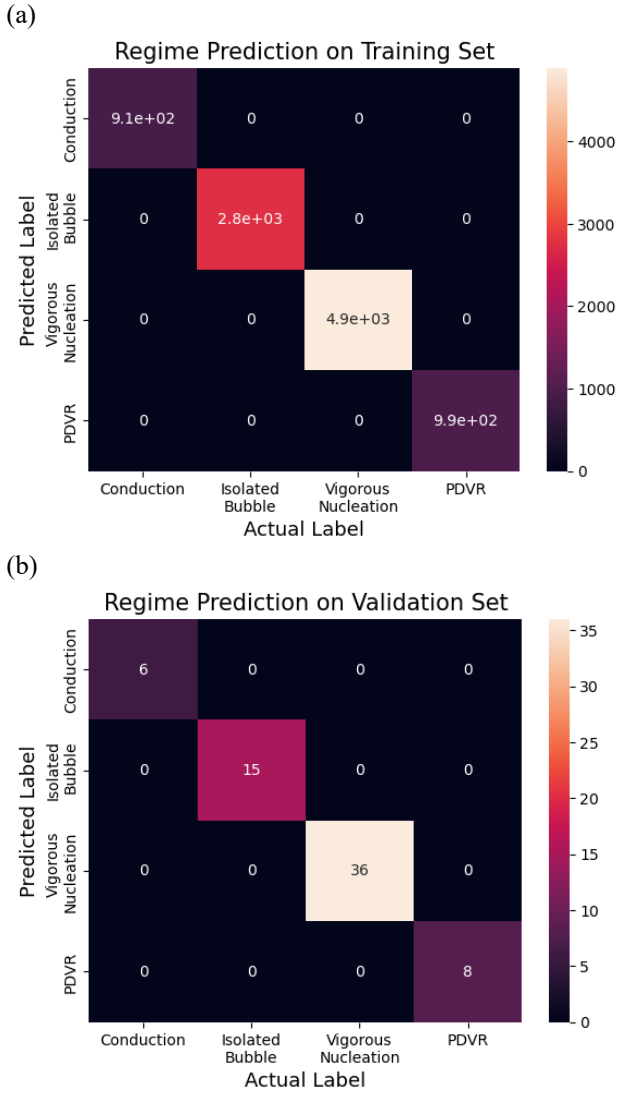

Fig. 11. Nucleation Regime prediction for Case II for (a) training dataset and (b) testing dataset

performance on the testing dataset was also 100% accurate. This is an indication that the
model has been able to successfully learn relevant patterns present in the image to make accurate classifications. The model was further analyzed for any distinct pattern on the data space using a stem plot of the predicted mean heat flux with its corresponding regime class. From the plot shown in Figure 12, we observed a similar pattern to that of the surface plot for model A i.e. the difference in mean heat flux along the droplet size axis seems to be more significant as the superheat temperature increases. Figure 13 shows a top view of this plot.

3. EXAMINING THE USE OF IMAGE DATA AS SUPERHEAT TEMPERATURE SENSOR FOR CASE II MODEL

In this section of the study, a new CNN model was trained to behave similarly to a temperature sensor. As shown in Figure 17, the architecture of the model developed here is very similar to that of Case I explored in the previous section. This architecture is configured to take a 100x100 array representation of the image data as input, and it generates the wall superheat temperature as output. The image data passes through a 3x3 convolution layer with 32 filters and a same padding. From here, a ReLU activation function is applied to this convolution output to introduce non-linearity. A 2x2 max pooling with a stride of 2 and a same padding is applied to summarize the feature captured by the convolution layer. This set of three operations is repeated one more time. As the data enters the fully connected region, the output from the convolution region is flattened. From here it passes through a dense layer with 32 neurons and a ReLU activation function. The data flows through an additional dense layer with 32 neurons and a ReLU activation function. From here, the data is connected to the final dense layer with one neuron outputting the superheat temperature.

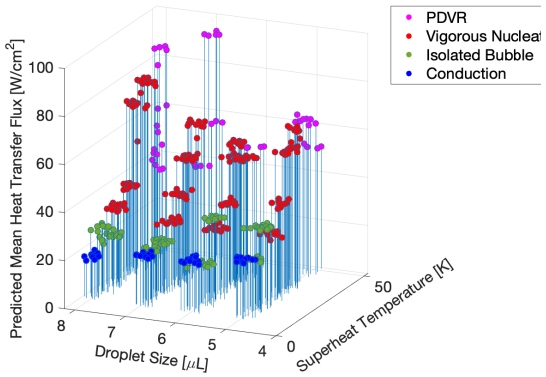

Fig. 12. Predicted Mean Heat Flux using Case II Model over the Entire Dataset.

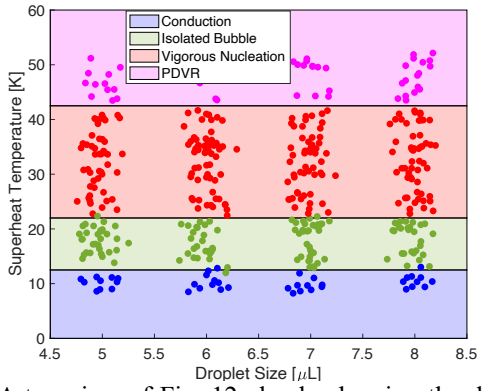

Fig. 13. A top view of Fig. 12 clearly showing the data points distribution over the different regimes.

Downloaded from http://asmedigitalcollection.asme.org/HT/proceedings-pdf/HT2025/88988/V001T03A006/7542844/v001t03a006-ht2025-156849.pdf by University of California Library - Berkeley user on 30 December 2025

Copyright © 2025 by ASME

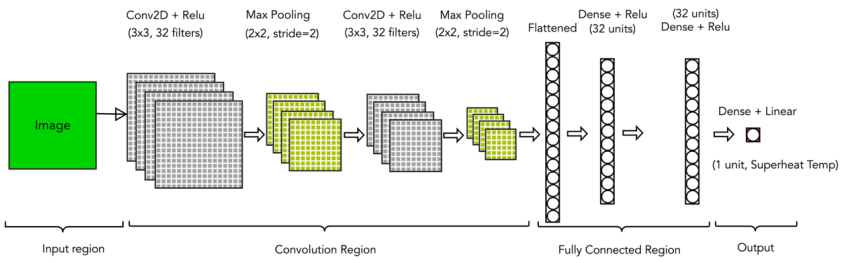

Fig. 14. CNN Architecture for Predicting Superheat Temperature from Image Only

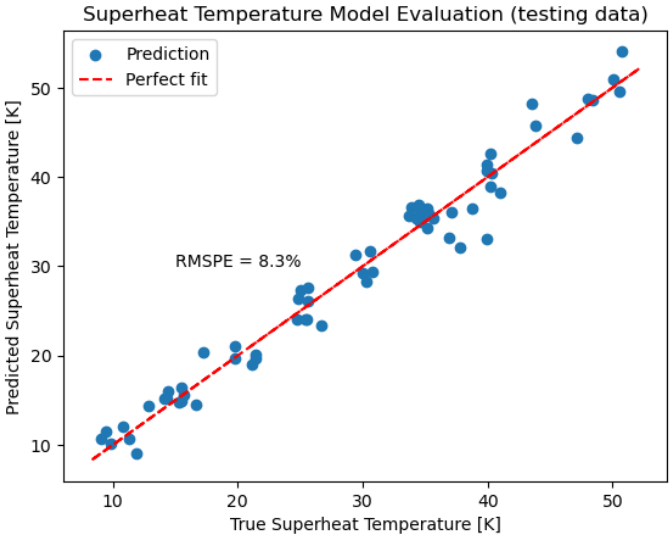

Fig. 15. Superheat Temperature Prediction for CNN model as a temperature sensor.

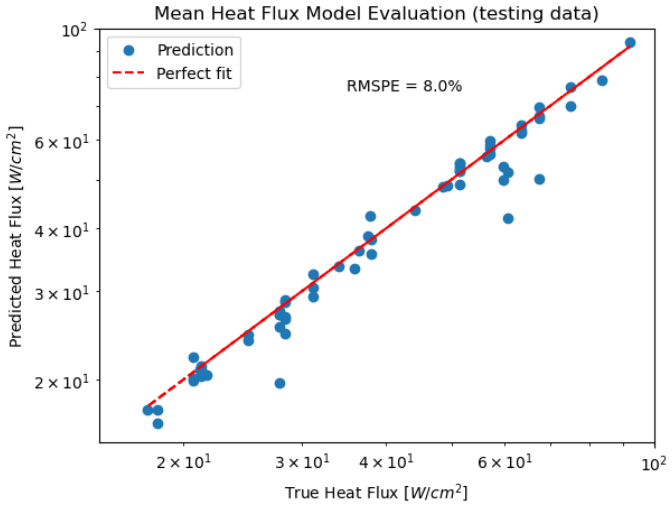

Fig. 16. Mean Heat Flux using Temperature Predicted from Image Only CNN Architecture

After training the CNN model using the same training dataset as the ones discussed in the previous section, we were able to get a superheat prediction with a RMSPE of 8.3% on the same testing dataset as the ones discussed in the previous section. Figure 15 depicts the observed result on the testing dataset. These predicted superheat temperatures are then applied to Case II model. Figure 16 shows the observed result of the Mean Heat flux as compared to the actual value. This prediction has a RMSPE of 8%. This result implies that a CNN model can be used as a temperature sensor for applications such as predicting mean heat flux.

4. COMPARING CASE RESULTS AND CONCLUSIONS

A convolution neural network can be a powerful tool with applications in many fields. In the field of boiling heat transfer, this tool can be used to capture information hidden in the regime morphology to predict the physical properties of a system including mean heat flux. Using the Python Keras functional API, it was possible to combine convolution layers and fully connected dense layers to produce a high-performing model capable of predicting the mean heat flux, superheat temperature, and morphology as needed.

Two models were developed throughout this study to better understand the potential of a trained CNN model on boiling heat transfer processes. The model developed for the simulated droplet images demonstrated the capability of taking array representations of images and relative pressure values as input to predict the morphology classes and superheat temperature values. All the observations in the testing dataset were accurately classified by the model and the superheat temperature prediction had a RMSPE of 12%. Using experimental data in two distinct cases, two models were produced with high predictive capabilities. In Case I the inputs were the droplet image, the droplet size, and the contact angle. These variables were used to predict the mean heat flux and superheat temperatures with a RMSPE of 10.2% and 9.1% respectively on the testing data set. The model developed in Case II was the best-performing model. The model takes a droplet image, droplet volume, contact angle, and superheat temperature as input values. These values are used to predict the nucleation regime and the mean heat flux. The nucleation regime had no misclassified out of 65 while the mean heat flux was predicted with a RMSPE of 7.3%.

Our results demonstrate that this model architecture can be trained to reliably predict the two-phase morphology regime and heat transfer performance from very low surface superheat elvels up to high superheat temperatures where partial dryout and vapor recoil are vividly observed. These demonstrate that the convolution neural network design, with a skip connection, developed in this study is a very effective convolution neural network (CNN) design that can be trained to predict boiling heat transfer performance with combined digital data and image information obtained in experiments. This type of modeling approach may be useful in a wide variety of boiling processes,

Downloaded from http://asmedigitalcollection.asme.org/HT/proceedings-pdf/HT2025/88988/V001T03A006/7542844/v001t03a006-ht2025-156849.pdf by University of California Library - Berkeley user on 30 December 2025

Copyright © 2025 by ASME

particularly for system geometries that may complicate the liquid-vapor morphology of the system. Our results also indicate that images of the boiling two-phase morphology during deposited droplet vaporization on superheated surfaces contain information about the process that correlates with the heat transfer performance. If the image information is included in training a CNN model, the image information overlaps with wall superheat information. We found that we could train the model to predict the vaporization mean heat flux with good accuracy using either the superheat or the image information. Using surface superheat information and image information combined improved model accuracy slightly in this case because the information in these two inputs is strongly (but not perfectly) correlated. The association of two-phase morphology with superheat level for pool boiling has been established empirically based on the trends and regimes in conventional boiling curves. Regimes (conduction-dominated pre-onset of nucleate boiling, fully-developed nucleate boiling, transition boiling, PDVR etc.) are generally acknowledged to correspond to specific ranges of surface superheat, each having a characteristic morphology. The study summarized here has demonstrated the correlation between surface superheat and morphology in a more direct way based on a data-science analysis. It has also demonstrated that our model architecture predictive capability can be extended to the PDVR regime resulting in trained predictive models with high accuracy. This approach may offer a means to explore boiling processes with more complicated physics.

ACKNOWLEDGEMENTS

This work is supported by the National Science Foundation through the Graduate Research Fellowship Program and NSF CBET grant number 2228373. Funding for this research was also provided by the endowment of the A. Richard Newton Chair in Engineering at UC Berkeley

REFERENCES

[1] Carey, V.P., Wemp, C.K., McClure, E.R., and Cabrera, S., 2018, "Mechanism Interaction During Droplet Evaporation on Nanostructured Hydrophilic Surfaces," paper IMECE2018-87991, *Proceedings of the ASME 2018 International Mechanical Engineering Congress and Exposition, IMECE2018*, November 9-15, 2018, Pittsburgh, PA.

[2] X.L. Wen, H.T. Wang, H. Wang, Prediction model of flow boiling heat transfer for R407C inside horizontal smooth tubes based on RBF neural network, *Procedia Eng.* 31(2012)233–239.

[3] A.M. Bahman, S.A. Ebrahim, Prediction of the minimum film boiling temperature using artificial neural network, *Int. J. Heat Mass Transf.* 155(2020) 119834.

[4] W.J. Wang, L.X. Zhao, C.L. Zhang, Generalized neural network correlation for flow boiling heat transfer of R22 and its alternative refrigerants inside horizontal smooth tubes, *Int. J. Heat Mass Transf.* 49(2006) 2458–2465.

[5] U. Sajjad, I. Hussain, C.C. Wang, A high-fidelity approach to correlate the nucleate Pool boiling data of roughened surfaces, *Int. J. Multiphase. Flow*, 142(2021) 103719.

[6] Y. Qiu, D. Garg, L. Zhou, C.R. Kharangate, S.M. Kim, I. Mudawar, An artificial neural Network model to predict mini/micro-channels saturated flow boiling heat transfer coefficient based on universal consolidated data, *Int. J. Heat Mass Transf.* 149(2020) 119211.

[7] A. Swain, M. Kumardas, Prediction of heat transfer coefficient in flow boiling over Tube bundles using ANFIS, *Exp. Heat Transfer* 37(5) (2016) 443–455.

[8] T. Cong, R. Chen, G. Su, S. Qiu, W. Tian, Analysis of CHF in saturated forced convective boiling on a heated surface with impinging jets using artificial neural network and genetic algorithm, *Nucl.Eng.Des*. 241 (2011) 3945–3951.

[8] A. Swain, M.K. Das, Artificial intelligence approach for the prediction of heat transfer coefficient in boiling over tube bundles, Proceedings of the Institution of Mechanical Engineers, Part C: *J. Mech. Eng. Sci*., 228(10) (2014) 1680–1688.

[10] M. Calati, G. Righetti, L. Doretti, C. Zilio, G.A. Longo, K. Hooman, S.Mancin, Water Pool boiling in metal foams: from experimental results to a generalized model based On artificial neural network, *Int. J. Heat Mass Transf*. 176(2021) 121451.

[11] Z.G. Xu, Z.G. Qu, C.Y. Zhao, W.Q. Tao, Experimental correlation for pool boiling heat transfer on metallic foam surface and bubble cluster growth behavior on grooved array foam surface, *Int. J. Heat Mass Transf*. 77(2014) 1169–1182.

[12] Z.Q. Long, P. Zhang, Heat transfer characteristics of thermosyphon with N2 –Ar binary mixture working fluid, *Int. J. Heat Mass Transf.* 63(2013) 204–215.

[13] Y. Kuang, F. Han, L. Sun, R. Zhuan, W. Wang, Saturated hydrogen nucleate flow boiling heat transfer coefficients study based on artificial neural network, *Int. J. Heat Mass Transf.* 175(2021)121406.

[14] N. Kishor, M.K. Das, Soft computing techniques for prediction of boiling heat transfer coefficient of liquids on copper-coated tubes. *Applied Artificial Intelligence,* 24(3), 2010, 24, 210–232. doi:10.1080/08839510903549614.

[15] McClure, E.R., and Carey, V.P., (October 13, 2021). Genetic Algorithm and Deep Learning to Explore Parametric Trends in Nucleate Boiling Heat Transfer Data, *ASME. J. Heat Transfer*. December 2021; **143**(12): 121602. https://doi.org/10.1115/1.4052435

[16] Tchouteng Njike, U., Cabrera, S., McClure, ER, and Carey, VP. "Use of Machine Learning Tools to Assess Surface Dryout

Downloaded from http://asmedigitalcollection.asme.org/HT/proceedings-pdf/HT2025/88988/V001T03A006/7542844/v001t03a006-ht2025-156849.pdf by University of California Library - Berkeley user on 30 December 2025

Copyright © 2025 by ASME

During Nucleate and Transition Boiling on Surfaces with Different Wetting and Substrate Properties." *Proceedings of the ASME 2021 Heat Transfer Summer Conference*. ASME. https://doi.org/10.1115/HT2021-64012

[17] Silva, A.D. and Carey, V.P., Use of A Genetic Algorithm to Model the Interaction of Conduction and Nucleate Boiling Mechanisms During Evaporation of Water Droplets on Superheated ZnO Nanostructured Surfaces, paper HT2023-107422, *Proceedings of the ASME 2023 Heat Transfer Summer Conference HT2023*, July 10-12, 2023, Washington, DC.

[18] Yang, B., Zhu, X., Wei, B., Liu, M., Li, Y., Lv, Z., and Wang, F., 2023, "Computer Vision and Machine Learning Methods for Heat Transfer and Fluid Flow in Complex Structural Microchannels: A Review," *Energies,* 16, 1500. https://doi.org/10.3390/en16031500

[19] Lee, M., 2022, "Optimized Experimental Observation and Measurements of Pool Boiling Heat Transfer Using Computer Vision Techniques," Master's Thesis, University of California, Irvine, ProQuest Dissertations Publishing, 28971170.

[20] Tchouteng Njike, U., and Carey, V.P., A Convolution Neural Network Design for Combined Image and Sensor Data Analysis to Determine Droplet Vaporization Regime and Heat Transfer Performance, paper SHTC2024-131218, *Proceedings of the ASME 2024 Heat Transfer Summer Conference HT2024*, July 15-17, 2024, Irvine, CA.

[21] Shorten, C., Khoshgoftaar, T.M. A survey on Image Data Augmentation for Deep Learning. *J Big Data,* 6, 60 (2019). https://doi.org/10.1186/s40537-019-0197-0

Downloaded from http://asmedigitalcollection.asme.org/HT/proceedings-pdf/HT2025/88988/V001T03A006/7542844/v001t03a006-ht2025-156849.pdf by University of California Library - Berkeley user on 30 December 2025

Copyright © 2025 by ASME